PUBLISHED BY IOP PUBLISHING FOR SISSA MEDIALAB

RECEIVED: *January 3, 2014*
REVISED: *January 28, 2014*
ACCEPTED: *January 31, 2014*
PUBLISHED: *March 7, 2014*

Single shot, temporally and spatially resolved measurements of fast electron dynamics using a chirped optical probe

J.S. Green,[a,1] **C.D. Murphy,**[b] **N. Booth,**[a] **R.J. Dance,**[c] **R.J. Gray,**[d] **D.A. MacLellan,**[d] **P. McKenna,**[d] **D. Rusby**[a] **and L. Wilson**[a]

[a] *Central Laser Facility, STFC, Rutherford Appleton Laboratory, Chilton, OX11 0QX, United Kingdom*
[b] *School of Physics and Astronomy, SUPA, University of Edinburgh, Mayfield Road, Edinburgh, EH9 3JZ, United Kingdom*
[c] *Department of Physics, York Plasma Institute, University of York, York, YO10 5DD, United Kingdom*
[d] *Department of Physics, SUPA, University of Strathclyde, Glasgow, G4 0NG, United Kingdom*

E-mail: james.green@stfc.ac.uk

ABSTRACT: A new approach to rear surface optical probing is presented that permits multiple, time-resolved 2D measurements to be made during a single, ultra-intense $\left(>10^{18}\,\mathrm{W\,cm^{-2}}\right)$ laser-plasma interaction. The diagnostic is capable of resolving rapid changes in target reflectivity which can be used to infer valuable information on fast electron transport and plasma formation at the target rear surface. Initial results from the Astra-Gemini laser are presented, with rapid radial sheath expansion together with detailed filamentary features being observed to evolve during single shots.

KEYWORDS: Plasma diagnostics - probes; Plasma diagnostics - interferometry, spectroscopy and imaging; Plasma generation (laser-produced, RF, x ray-produced); Plasma diagnostics - high speed photography

[1] Corresponding author.

doi:10.1088/1748-0221/9/03/P03003

Contents

2014 JINST 9 P03003

1 Introduction

The study of fast electron transport in solid targets is crucial for many key applications, yet the ability to diagnose various transport processes within the target remains an issue. A number of experiments have worked to address the challenge of diagnosing fast electron beam temperature, number density and beam divergence. Of these, both diagnosing and controlling the fast electron beam divergence is perhaps the greatest challenge.

The first studies of fast electron transport used transverse optical probing of the target rear surface was used to infer a fast electron distribution at the rear of the target [1], with OTR used to measure the highest energy electrons as they leave the target rear surface [2]. Complementary measurements of optical probing combined with Cu K-α and XUV imaging inferred [3] a large fast electron divergence angle ($> 50^{\circ}$) in a ballistic transport regime, with Green et al. [4] observing that the fast electron divergence angle increases with laser intensity when a broad range of diagnostic techniques is considered.

Studies of Target Normal Sheath Acceleration (TNSA) of protons and ions, namely measurements of the rear surface ion source size, have also been used to diagnose fast electron distribution and subsequent sheath field evolution [5]. However as the target thickness, d, reduces to the order of the pulse length , τ, ($d < c\tau$) the rapid transverse expansion (close to c) of the accelerating sheath fields [6, 7], typically attributed to electron recirculation or spreading of the charge distribution on the target rear surface, can lead to an ion source size much larger than that which might be expected from even the most divergent fast electron beam.

Temporally resolving the formation of these intense sheath fields, that form at the very earliest stages of the interaction, could yield important data on the initial fast electron population. In addition when used in conjunction with ion source size measurements this technique could be used to temporally probe the plasma expansion dynamics that result in high energy ion production, for which not a lot is currently known for short pulse ($< 100\,\mathrm{fs}$) laser systems.

2 Target reflectivity

The characteristic formation of a plasma at the target rear surface during TNSA, on the order of the Debye length, is mainly a result of field-induced barrier suppression (FIBS) ionisation that occurs rapidly under the influence of intense TV/m electric fields [8]. Careful measurements of the modified reflectivity profile on the target rear surface can be used to temporally-resolve sheath formation, permitting crucial measurements of the initial, and late time, fast electron distribution to be made.

Light incident on to a polished, metallic surface (Al will be considered in this paper) would reflect off as governed by Fresnel's law. In this case the reflectivity of the surface at a fixed angle of incidence is determined by the complex refractive index given by:

$$n^2 = \frac{c^2k^2}{\omega^2} = \epsilon + \frac{4\pi\sigma}{\omega}i \tag{2.1}$$

where k is the wave number, ϵ is the electric permittivity, σ is the electrical conductivity and ω is the laser angular frequency.

With the formation of a localised plasma at the slab surface, how the target reflectivity is calculated is largely dependent on the plasma scalelength, l, $\big($exponential electron number density profile, $n = n_0 \exp(-x/l)\big)$. In the case of a perfect, step-like interface between the Al slab and the vacuum, or a very steep scalelengh $l \ll \lambda$ (where λ is the wavelength of the probe laser) the fraction of laser light reflected can still be calculated from the Fresnel equations, with the electrical conductivity, $\sigma(\omega)$, largely determining the level of reflectivity:

$$\sigma(\omega) = \frac{\omega_p^2}{4\pi(1/\tau_e i - i\omega)} \tag{2.2}$$

where ω_p is the plasma frequency and $\tau_e i$ is the electron-ion collision frequency.

However when a modest plasma expansion occurs ($l \approx \lambda$) the standard Fresnel equations are no longer valid. Instead the laser light propagates through a plasma density gradient until it reaches the critical density surface, at which point the light is reflected. Calculating the fraction of laser light absorbed and reflected requires solving Maxwell's equations for light propagating through a known plasma density gradient at a defined angle of incidence. Celliers et al. [9] used the standard Drude model together with Maxwell's equations to calculate the reflectivity of an optical probe propagating through a range of shock-heated plasma gradients. The authors found clear dependences of the reflectivity on the laser wavelength, polarization and angle of incidence. Despite a range of plasma scalelengths being investigated, the largest fraction of laser reflection and absorption was always found to occur at the critical density layer. In their study the authors found resonant absorption of the laser at the critical density to be the dominant form of energy loss from the pulse although inverse Bremsstrahlung would also be expected to be a significant absorption mechanism for low laser intensities $\left(< 10^{15}\,\mathrm{W\,cm^{-2}}\right)$.

Benuzzi et al. [10]applied this method experimentally to study the change in optical reflectivity of plain Al targets when subject to X-ray pre-heating and laser-driven shocks generated by a modest laser intensity of $6 \times 10^{13}\,\mathrm{W\,cm^{-2}}$. X-ray pre-heating of the rear surface was seen to lead to a marked drop in reflectivity from 90% to 60% over $\sim$100 ps.

2014 JINST 9 P03003

Antici et al. [11, 12] extended the technique to look at hot electron dynamics for higher intensity interactions $\left(5 \times 10^{19}\,\mathrm{W\,cm^{-2}}\right)$. The authors probed the target rear surface with ~ 4 ps resolution, making 1D spatial measurements of the probe's phase in order to extract data on the shape of the plasma expansion and fast electron distribution. Changes to the phase of the optical probe were used to determine both the hot and cold electron population as a function of radius on the rear of the target. The analysed data revealed a bell-shaped electron distribution that was observed in both the hot electron density and cold (bulk) electron temperature. Similar spatial distributions would be expected as energy is transferred locally between the fast and bulk electron populations, via either collisional or resistive heating.

In this paper we present a new approach to rear surface optical probing that permits multiple, time-resolved 2D measurements to made for a single shot with a high degree of spatial and temporal precision. By studying changes in reflectivity across the whole target surface, the structure and evolution of the electron distribution can be studied for a range of laser and target parameters, even for cases where non-uniform or highly asymmetric structures are expected.

3 Diagnostic outline

For many experiments it is preferable to probe at multiple time steps on a single shot rather than perform a delay scan over many shots. In order to achieve this the optical probe can be temporally chirped and the collected light imaged onto an optical spectrometer [11]. This method gives a direct relation between optical frequency and time. Although it should be noted that the time resolution of the system Δt is typically limited not by the spectral resolution of the spectrometer but by the relation [13]:

$$\Delta t = \sqrt{\tau_0 \times \tau_c} \tag{3.1}$$

where τ_0 and τ_c are the bandwidth-limited and chirped pulse durations respectively.

Here we present a novel implementation of rear surface optical probing that for the first time yields multiple, temporally-resolved, 2D images from a single shot by using a spectral filtering method. In order to achieve temporal separation the probe beam was linearly chirped, with the bandwidth of the laser being used to relate wavelength with probing time as usual. However, rather than using a spectrometer, the collected probe light from the target was split between three CCD cameras, each having a different narrow-pass filter in place to isolate one section of the linear chirp. By using this technique, rather than an optical spectrometer, we were able to obtain three different snapshots in time complete with 2D spatial information. The spectral bandwidth of the optical filters used when demonstrating this technique are shown in figure 1, along with the bandwidth of the Astra Gemini laser which was used to both irradiate and probe the target foils.

Astra Gemini, based at the Central Laser Facility, is a dual-beam Ti:Sapphire 800 nm laser that delivers 10 J of energy on target per beam with a pulse duration of 45 fs. In order to test this new method of optical probing one of these beams was focused on to target at 30 degrees incidence using an f /2 parabola resulting in a Full Width Half Maximum (FWHM) spot size of 2.5 μm. Approximately 30% of the incident laser energy was contained within the central focal spot, resulting in a peak intensity of $\sim 10^{21}\,\mathrm{W\,cm^{-2}}$.

For the rear surface optical probe the other arm of Astra Gemini was chirped from 45 fs to 0.3–5 ps by detuning the compressor, equating to a maximum temporal resolution of 100 fs. The

2014 JINST 9 P03003

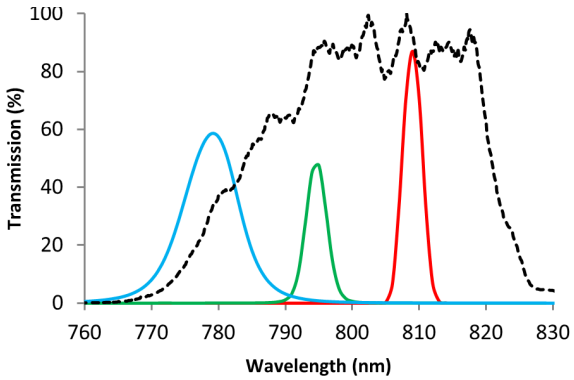

Figure 1. Transmission spectra of optical filters (coloured lines) used to isolate narrow portions of the Astra Gemini spectrum (dashed line). Using the linear chirp of the beam, each filter effectively selects a narrow time window for observation.

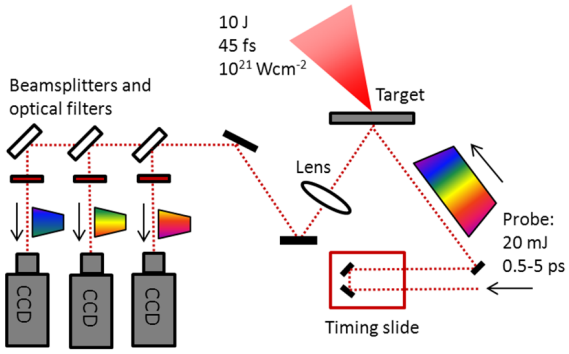

Figure 2. Astra-Gemini diagnostic layout showing the chirped optical probe reflecting off the target rear surface before being imaged onto three CCD cameras, each filtered to view a specific wavelength range and hence temporal snapshot.

p-polarised beam was then apodised down to 10 mm and directed on to the target rear surface at an angle of 40 degrees (relative to target normal) (see figure 2). Light reflected from the target rear surface was collected using a f = 40 cm achromatic lens and imaged onto three CCD cameras, with a total magnification of $\times 7$ and a spatial resolution of 6 μm. Each CCD camera had a different interference filter mounted in front of the chip, with central wavelengths of 780 nm, 795 nm and 808 nm, with 780 nm corresponding to start of the probe pulse and 808 nm the tail.

The timing of the optical probe relative to the main interaction pulse was varied with the use of a remote timing slide. The t = 0 point was established by focusing the main pulse in air at low intensity and altering the relative timing of the probe beam until the initial plasma formation was just visible. With a non-normal angle of incidence on target (40 degrees in the horizontal plane in this case), it is worth noting that the precise timing of the probe relative to the interaction pulse varies across the horizontal axis. For a target foil of 1 mm diameter, probe light incident on one edge of the target foil would arrive approximately 2 ps before that illuminating the opposite edge, hence you would expect to see an earlier profile of the sheath evolution as you look from one side of the target to the other. For quick measurements of radial sheath expansion on the rear surface vertical line-outs can be taken but the horizontal temporal gradient could be used to extract additional temporal information if carefully deconvolved.

2014 JINST 9 P03003

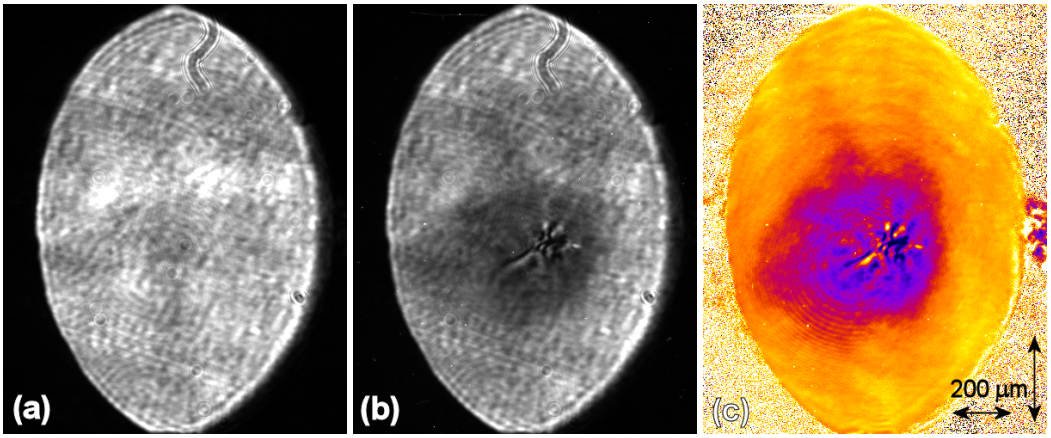

Figure 3. Rear surface optical probe images of a 50 μm Al foil: (a) Before shot (b) 5 ps after main interaction (c) normalised reflectivity profile 5 ps after main interaction, with lighter (yellow) shades indicating high reflectivity, comparable to the original solid aluminium conditions, and darker (purple) shades indicating absorption by the plasma surface.

The probe pulse contained approximately 20 mJ of energy, with a maximum intensity on target of $5 \times 10^{10}\,\mathrm{W\,cm^{-2}}$. At this intensity the probe beam itself is not sufficiently intense to modify the reflectivity of the target surface, with intensities $> 10^{10}\,\mathrm{W\,cm^{-2}}$ typically required to increase the Al resistivity in order to bring about a measurable change in reflectivity [14]. Hence any observed change in reflectivity is due to the separate, high intensity interaction pulse. In addition, since Astra Gemini is capable of firing each beam line independently, it is possible to fire just the probe beam on its own. This was done a number of times on thin (100 nm) foil targets in order to confirm that the probe pulse had no adverse affect on the target surface quality. In addition, the dual beam set-up also provides an ideal way of verifying the position and surface quality of the target prior to the shot, and crucially allows a direct, normalised comparison to be made with the post-shot image.

4 Initial results

Here we present some initial results using the single-shot, time-resolved rear surface optical probe in order to demonstrate the applicability of the new technique. A number of Al target foils were irradiated during the course of the experiment, with thicknesses varying from 100 nm to 150 μm. Each target foil was mounted in a 5×5 array, with a 1 mm clear circular aperture for each target position.

Figure 3 illustrates the process of generating 2D reflectivity profiles. The left hand image shows the reference image of the target foil before the main interaction. The centre image shows the same foil, but imaged 5 ps after the main interaction at the target front surface, with a temporal resolution of 1.5 ps. The right hand image combines both images to generate a reflectivity map at that time, isolating the regions of the target where the reflectivity has changed, thus making it easier to analyse.

The three temporally resolved reflectivity profiles from this first shot are shown in figure 4 at times of +5, +6.5 and +8 ps. Figure 4 shows a large ($\sim$250 μm diameter) region of lower reflectivity that expands radially outwards, with the average reflectivity dropping from 40% to 30% within the

2014 JINST 9 P03003

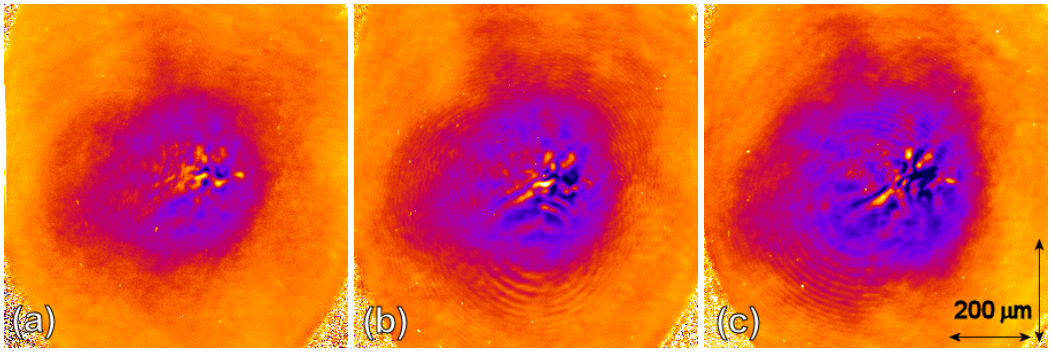

Figure 4. Central detail of rear surface reflectivity profile for a single shot on a 50 μm Al foil (a) 5 ps (b) 6.5 ps and (c) 8 ps after the main interaction. Note the viewing angle of the target means that the horizontal dimension is contracted.

bounds of the feature over 3 ps. In the central region of lower reflectivity, several filamentary-type structures can be seen with features on a scale of $\sim$10 μm (see figure 4). Within these structures reflectivity falls to below 20%, suggesting that the probe light is either being strongly absorbed or refracted / scattered out of the cone angle of the collection optic.

Further studies will investigate the exact source of this radial expansion but the observed decrease in reflectivity with time is consistent with fast electron-sourced plasma formation at the target rear surface. As the plasma expands into the vacuum the change from a step-like density profile to a finite scale length at the critical surface would lead to increased coupling of probe light into the plasma. In the region of the laser focal spot, where filamentary-type structure is observed, a greater flux of high energy electrons on axis would be expected to seed instabilities that would grow rapidly during the laser pulse length, leading to some break-up of the beam inside the target. Such instabilities would lead to strong modulations in the electron density at the target rear surface, which can be seen imprinted into the sheath profile in figure 4.

As expected a small degree of horizontal asymmetry is observed in the three time resolved profiles that isn't seen in the vertical axis. This is attributed to the spread of probe timings as mentioned in section 3. From the reader's perspective probe light incident on the far right edge of the target foil would arrive approximately 2 ps before that illuminating the far left hand edge, hence you would expect to see an earlier profile of the sheath evolution as you look from left to right.

Applying this probing technique to thin foil targets (100 nm Al) in a higher temporal resolution regime ($\Delta t = 300$ fs) reveals similar features (figure 5) to that of the 50 μm foil. Detail close to the interaction point is partly masked by a bright coherent transition radiation (CTR) signal that results from the highest energy electrons crossing the plasma-vacuum boundary [2]. Inset into the two reflectivity profiles of figure 5 are filtered images of this central region, showing spatial detail of the time-integrated CTR signal. Whilst additional filtering can be added to measure the CTR spatial distribution, yielding extra data on the highest energy fast electrons, removing such a bright signal from the time-resolved reflectivity measurements is difficult. CTR effects can be mitigated by shooting thicker targets, or using a lower intensity drive laser, however for the thinnest (nm) foils an off-harmonic probe is required to move the wavelength range of interest away from the first and second laser harmonic.

2014 JINST 9 P03003

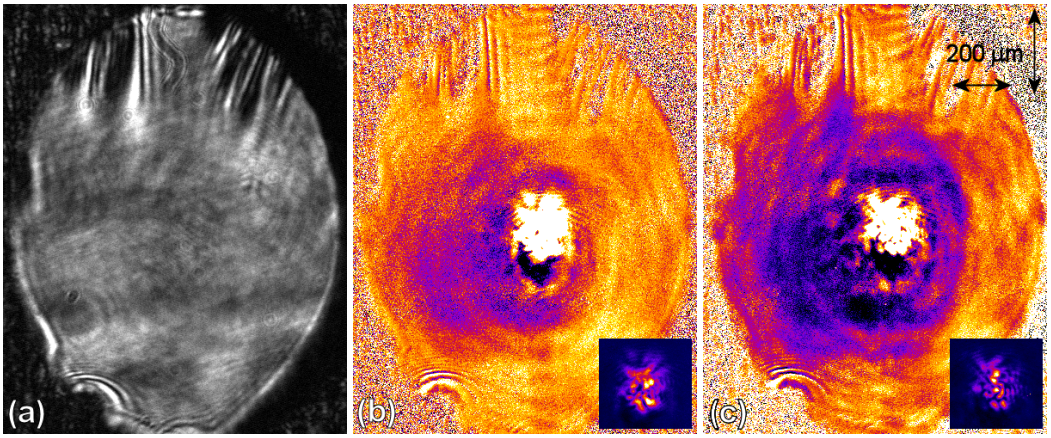

Figure 5. (a) Rear surface probe reference image for a 100 nm Al foil before the main interaction. Significant defects in the foil structure can be identified and the target moved / changed accordingly. Reflectivity profile (b) 2.2 ps and (c) 2.5 ps after the main interaction. Inset into the reflectivity maps is filtered detail of the bright transition radiation signal at the centre of each image. Note the viewing angle of the target means that the horizontal dimension is contracted.

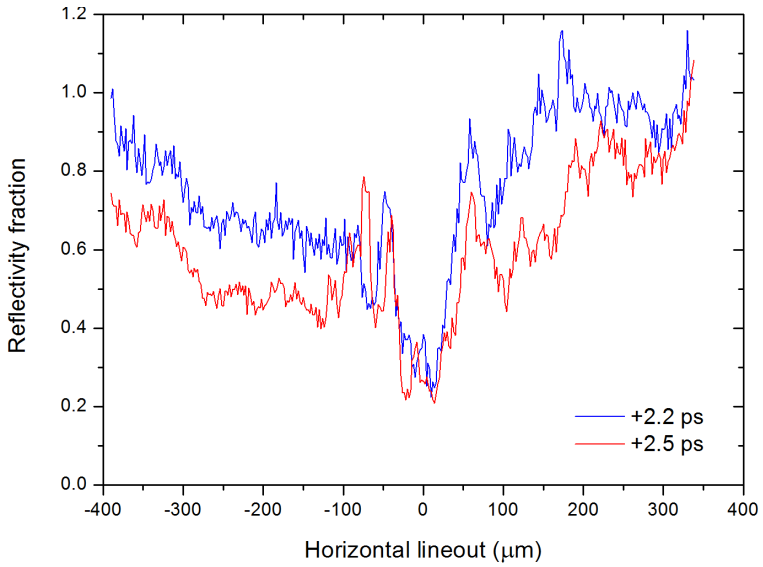

Figure 6. Horizontal line outs of the rear surface reflectivity plots shown in figure 5, taken just below the interaction point 2.2 and 2.5 ps after the main interaction. 0 μm marks the position of the laser focus.

Outside of the central interaction region the short (300 fs) separation between the two reflectivity profiles shown in figure 5 permits rapidly expanding features to be resolved that would not be resolved with lower, picosecond resolution. Similar to the 50 μm foil, a diffuse outer region of low reflectivity $(40-70\%)$ is observed with a dark central zone where very little probe light is seen $(<20\%)$.

Figure 6 shows a horizontal line-out of the reflectivity profiles from figure 5 taken just below the central interaction axis (in order to minimise CTR counts). A drop in reflectivity of almost 20% can be seen over 300 fs, demonstrating a rapid change in the plasma density profile at the target rear surface. However in the central interaction region the minimum reflectivity of 20% is

2014 JINST 9 P03003

not seen to decrease, suggesting a minimum threshold below which the majority of laser light is being absorbed, or scattered out of the collection optics. Future implementations of this diagnostic could include a plastic screen around the primary collection optic in order to look for any scattered light that is reflected from the target. For such a thin target it is also possible that decompression of the target either during or just before the peak of the main interaction pulse may lead to the plasma density close to the laser focal spot becoming under-critical, thus allowing probe light to propagate through the foil.

When comparing this new technique with that previously demonstrated by Antici et al. [11, 12], consideration needs to be given to both the experimental measurements required from each shot and the diagnostic resources available. In the case of a probe beam with a large chirp with a relatively high temporal resolution, maximum temporal information would be extracted with the use of a spectrometer (where the use of many CCD cameras and optical filters may be deemed impractical). However when temporal resolution is relatively low compared to the temporal chirp, as is the case in this paper, the option of imaging multiple 2D snapshots of the target rear surface is greatly advantageous. The additional spatial information obtained is often crucial in characterising complex laser-plasma interactions where circular symmetry can rarely be assumed. Pre-shot target characterisation is also very important when analysing experimental data of this kind, and our novel approach to rear surface probing permits full 2D characterisation of the target foil surface quality, permitting us to clearly resolve any abnormal target features that might complicate data analysis once the main interaction has occurred.

The phase measurements outlined by Antici et al. have the capability to provide supplemental information that absolute reflectivity measurements cannot in isolation. However the addition of a Mach-Zehnder interferometer could easily add such a capability to our 2D approach, with the benefit of an extra spatial dimension. This would be crucial when dealing with a significant non-uniform, asymmetric sheath expansion on the target rear surface, as is often observed experimentally. Such an approach will be implemented on an upcoming experiment.

5 Conclusion

A novel method of temporally and spatially resolving sheath formation on the rear surface of targets has been implemented. By utilising the broad bandwidth of a Ti:Saphire laser, a chirped optical probe in conjunction with a number of narrowband interference filters was used to record multiple 2D, time-resolved images on a single shot. With spatial resolution of 6 μm and variable temporal resolution of 100 fs–1.5 ps, the diagnostic is capable of resolving rapid changes in target reflectivity which can be used to infer valuable information on fast electron transport and plasma formation at the target rear surface.

From single shots on the Astra-Gemini laser a rapidly expanding region of low reflectivity was seen on the rear surface of a 50 μm Al foil, and fine structured filamentary features resolved over several picoseconds. With a temporal window of just 300 fs, the earliest stages of plasma formation at the rear of 100 nm Al foils was seen. Future developments will see not only higher spatial and temporal resolution, but the addition of an interferometry channel in order to characterize the plasma density scale lengths alongside existing reflectivity measurements. This would permit a more detailed measurement of the plasma expansion and analysis in order to resolve the very earliest stages of fast electron dynamics at the target rear surface.

2014 JINST 9 P03003

Acknowledgments

The authors would like to thank the staff at the Central Laser Facility for all of their valuable assistance during the experimental campaign. This work was supported by the EPSRC (grant number EP/J003832/1).

References

[1] M. Tatarakis et al., *Plasma Formation on the Front and Rear of Plastic Targets due to High-Intensity Laser-Generated Fast Electrons*, *Phys. Rev. Lett.* **81** (1998) 999.

[2] J.J. Santos et al., *Fast Electron Transport in Ultraintense Laser Pulse Interaction with Solid Targets by Rear-Side Self-Radiation Diagnostics*, *Phys. Rev. Lett.* **89** (2002) 025001.

[3] K.L. Lancaster et al., *Measurements of energy transport patterns in solid density laser plasma interactions at intensities of* 5×10^{20} Wcm^{-2}, *Phys. Rev. Lett.* **98** (2007) 125002.

[4] J.S. Green et al., *Effect of laser intensity on fast-electron-beam divergence in solid-density plasmas*, *Phys. Rev. Lett.* **100** (2008) 015003.

[5] T.E. Cowan et al., *Ultralow Emittance, Multi-MeV Proton Beams from a Laser Virtual-Cathode Plasma Accelerator*, *Phys. Rev. Lett.* **92** (2004) 204801.

[6] P. McKenna et al., *Lateral electron transport in high-intensity laser-irradiated foils diagnosed by ion emission*, *Phys. Rev. Lett.* **98** (2007) 145001.

[7] K. Quinn et al., *Laser-driven ultrafast field propagation on solid surfaces*, *Phys. Rev. Lett.* **102** (2009) 194801.

[8] M. Hegelich et al., *MeV Ion Jets from Short-Pulse-Laser Interaction with Thin Foils*, *Phys. Rev. Lett.* **89** (2002) 085002.

[9] P. Celliers et al., *Optical probing of hot expanded states produced by shock release*, *Phys. Rev.* **E 47** (1993) 3547.

[10] A. Benuzzi et al., *Preheating study by reflectivity measurements in laser-driven shocks*, *Phys. Plasmas* **5** (1998) 2410.

[11] A. Antici et al., *Time and space resolved interferometry for laser-generated fast electron measurements*, *Rev. Sci. Instrum.* **81** (2010) 113302.

[12] A. Antici et al., *Hot and cold electron dynamics following high-intensity laser matter interaction*, *Phys. Rev. Lett.* **101** (2008) 105004.

[13] J.-P. Geindre et al., *Single-shot spectral interferometry with chirped pulses*, *Opt. Lett.* **26** (2001) 1612.

[14] H.M. Milchberg, R.R. Freeman, S.C. Davey and R.M. More, *Resistivity of a Simple Metal from Room Temperature to* 10^6 K, *Phys. Rev. Lett.* **61** (1988) 2364.

2014 JINST 9 P03003